Journal of Magnetic Resonance 228 (2013) 95–103

Contents lists available at SciVerse ScienceDirect

Journal of Magnetic Resonance

journal homepage: www.elsevier.com/locate/jmr

A more accurate estimate of T_2 distribution from direct analysis of NMR measurements

Fred K. Gruber [a], Lalitha Venkataramanan [a,*], Tarek M. Habashy [a], Philip M. Singer [b], Denise E. Freed [a]

[a] Schlumberger-Doll Research, One Hampshire Street, Cambridge, MA 02139, United States
[b] Schlumberger Reservoir Sampling and Analysis, 6350 W. Sam Houston Pkwy N., Suite 200, Houston, TX 77041, United States

ARTICLE INFO

Article history:
Received 24 September 2012
Revised 16 December 2012
Available online 9 January 2013

Keywords:
Nuclear magnetic resonance
Inverse problems
Regularization
Moments
Mellin transform

ABSTRACT

In the past decade, low-field NMR relaxation and diffusion measurements in grossly inhomogeneous fields have been used to characterize pore size distribution of porous media. Estimation of these distributions from the measured magnetization data plays a central role in the inference of insitu petro-physical and fluid properties such as porosity, permeability, and hydrocarbon viscosity.

In general, inversion of the relaxation and/or diffusion distribution from NMR data is a non-unique and ill-conditioned problem. It is often solved in the literature by finding the smoothest relaxation distribution that fits the measured data by use of regularization.

In this paper, estimation of these distributions is further constrained by linear functionals of the measurement that can be directly estimated from the measured data. These linear functionals include Mellin, Fourier–Mellin, and exponential Haar transforms that provide moments, porosity, and tapered areas of the distribution, respectively.

The addition of these linear constraints provides more accurate estimates of the distribution in terms of a reduction in bias and variance in the estimates. The resulting distribution is also more stable in that it is less sensitive to regularization. Benchmarking of this algorithm on simulated data sets shows a reduction of artefacts often seen in the distributions and, in some cases, there is an increase of resolution in the features of the T_2 distribution. This algorithm can be applied to data obtained from a variety of pulse sequences including CPMG, inversion and saturation recovery and diffusion editing, as well as pulse sequences often deployed down-hole.

1. Introduction

In oilfield applications, the measured NMR magnetization data denoted by $G(t)$ is a multi-exponential decay, with time constant T_2 and amplitudes $f(T_2)$,

$$G(t) = \int_0^\infty e^{-t/T_2} f(T_2) dT_2 \tag{1}$$

The transverse relaxation time T_2 is the characteristic time corresponding to a loss of coherance by protons in hydrocarbons or water present in pores of a rock or in the bulk fluid [1].

In (1), the T_2 distribution, denoted by $f(T_2)$, is estimated from the measured data $G(t)$. The conventional approach to estimating $f(T_2)$ is based on the inverse Laplace transform (ILT) [2]. However, it is well-known that the ILT is an ill-posed problem and has a non-unique solution and a large sensitivity to noise in the measurement [3,4]. The classical solution to this problem involves the introduction of a regularization functional, resulting in the minimization of a cost function Q with respect to the underlying distribution f,

$$Q = \|G - Lf\|^2 + \alpha \|f\|^2 \tag{2}$$

where G is the measured magnetization data, L is the matrix of the discretized kernel e^{-t/T_2}, and f is the discretized version of the underlying density function $f(T_2)$. The first term in the cost function is the least squares error between the data and the fit from the model in (1). The second term is referred to as the regularization and incorporates smoothness in the relaxation amplitudes into the problem formulation. The parameter α denotes the compromise between the fit to the data and an *a priori* expectation of the distribution. In (2), α is the weight given to the regularization and can be chosen by a number of different methods [5].

Recently, it has been shown that an integral transform approach can be used to estimate linear functionals of the T_2 distribution directly from the data without the need of regularization [6]. The central idea of this approach is to compute the integral transform of $G(t)$ using a kernel $k(t)$ such that the Laplace transform of $k(t)$ denoted by $K(T_2)$ has the desired properties in the T_2 domain.

* Corresponding author.
E-mail address: lvenkataramanan@slb.com (L. Venkataramanan).

1090-7807/$ - see front matter © 2013 Elsevier Inc. All rights reserved.
http://dx.doi.org/10.1016/j.jmr.2012.12.008

Let the integral transform of the data $G(t)$ be denoted by $\mathcal{L}\{G(t)\} = A$. It is defined as

$$\mathcal{L}\{G(t)\} = A \equiv \int_0^\infty k(t)G(t)dt \tag{3}$$

From (1) and (3),

$$A = \int_0^\infty K(T_2)f(T_2)dT_2 \tag{4}$$

where the functions $k(t)$ and $K(T_2)$ form a Laplace-transform pair, with

$$K(T_2) \equiv \int_0^\infty k(t)e^{-t/T_2}dt \tag{5}$$

Thus for a desired linear transformation $K(T_2)$ in the T_2 domain the integral transform approach constructs a kernel $k(t)$ in the time-domain, so that the scalar product of the kernel with the measured data provides A, the parameter of interest.

An advantage of this approach is the direct computation of linear functionals of the T_2 distribution without use of the ILT method. For example, the moments of the T_2 distribution, defined as

$$\langle T_2^\omega \rangle \equiv \int_0^\infty T_2^\omega f(T_2)dT_2$$

can be estimated from the Mellin transform of the magnetization data according to (for details of the implementation see [7]):

$$\langle T_2^\omega \rangle = \frac{(-1)^n}{\phi\Gamma(\mu)} \int_0^\infty t^{\mu-1}\left[\frac{d^nG(t)}{dt^n}\right]dt \tag{6}$$

$$\omega = \mu - n, \quad \text{with} \begin{cases} n = 0, & \text{if } \omega > 0 \\ n = [-\omega] + 1 & \text{otherwise} \end{cases} \tag{7}$$

where ϕ is the area under the T_2 distribution. Similarly, the tapered areas, defined as

$$B = \int_0^\infty K(T_2, T_c)f(T_2)dT_2 \tag{8}$$

were $K(T_2, T_c)$ is a desired transition function, e.g.,

$$K(T_2, T_c) = \frac{0.7213T_2}{T_c}\tanh\left(\frac{\alpha}{T_2}\right) \tag{9}$$

can be estimated by means of the exponential Haar transform (EHT) [6]

$$B = \int_0^\infty k(t, T_C)G(t)dt$$

with

$$k(t, T_c) = C(-1)^n e^{-\beta t}, \quad 2n\alpha < t < 2(n+1)\alpha \tag{10}$$

where $C = 0.7213/T_c$, $\alpha = 1.572T_c$, $\beta = 0.4087/T_c$, and $\gamma = 1/T_2 + \beta$. An extensive table of tapered areas transforms and their properties is given in [6].

An additional advantage of this approach is that since the transformation is linear, it is possible to estimate the uncertainty in the parameters. Let the discretized version of the linear transform be denoted by

$$A = k^T G$$

where k is the discretization of the $k(t)$ in (3) and G refers to the discretization of the measured data. Let σ_ϵ^2 be the variance of the vector of measurements G due to the Gaussian noise. Then the variance of A is given by

$$\sigma_A^2 = \sigma_\epsilon^2\|k\|^2 \tag{11}$$

In general, parameters obtained using the integral transform tend to have a smaller bias than those obtained using the standard ILT and are estimated without the need of a regularization term [6,7]. This approach also provides reasonable estimates of the associated parameter uncertainty as a function of signal-to-noise ratio (SNR) in the data. Therefore, these estimates are good candidates to be considered as additional priors in the estimation of the T_2 distribution.

In the new algorithm proposed in this paper, referred to as ILT+, we propose including specific linear functionals (associated to moments and tapered areas of the T_2 distribution) as additional constraints to estimate the T_2 distribution from the measured data. These linear constraints can be included into the problem formulation in a number of ways. We demonstrate one such method below with constraints from moments and areas being included in the problem formulation.

2. New algorithm for estimating the T_2 distribution: ILT+

Let G be a vector containing the measurements and L be a matrix representing the discretization of the kernel in (1). Assume that N_m moments, denoted by $\langle T_2^{\omega_i}\rangle, i = 1, \ldots, N_m$ and N_a areas, denoted by $B_i, i = 1, \ldots, N_a$ are estimated directly by means of the appropriate integral transforms on $G(t)$ (e.g., Eqs. (6)–(9)). The ILT+ algorithm involves minimizing a cost function with respect to $f(T_2)$,

$$\min_{f\geqslant 0}\left\|W(\overline{G} - \overline{L}f)\right\|^2 + \alpha\|f\|^2 \tag{12}$$

where

$$\overline{G} = \begin{bmatrix} G \\ \langle T_2^{\omega_1}\rangle \\ \vdots \\ \left\langle T_2^{\omega_{N_m}}\right\rangle \\ B_1 \\ \vdots \\ B_{N_a} \end{bmatrix} \tag{13}$$

is an extended vector containing the measurements and two constraints: the moments and the areas. $\overline{L}$ is the extended matrix,

$$\overline{L} = \begin{bmatrix} L \\ \begin{pmatrix} \frac{1}{\phi}T_{2,min}^{\omega_1} & \cdots & \frac{1}{\phi}T_{2,max}^{\omega_1} \\ \vdots & \ddots & \vdots \\ \frac{1}{\phi}T_{2,min}^{\omega_{Nm}} & \cdots & \frac{1}{\phi}T_{2,max}^{\omega_{Nm}} \end{pmatrix} \\ K(T_2, T_{c_1}) \\ \vdots \\ K(T_2, T_{c_{N_a}}) \end{bmatrix} \tag{14}$$

where L is a matrix with components

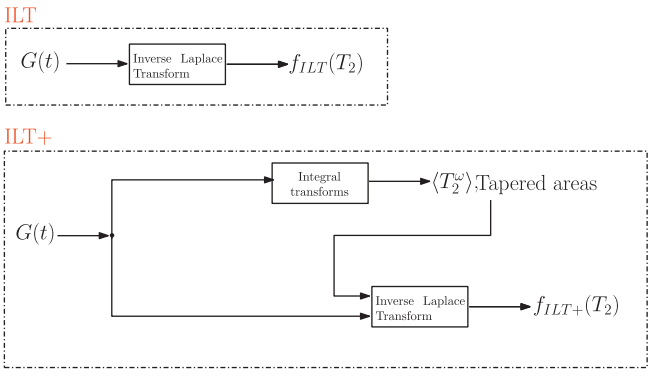

Fig. 1. Workflow of ILT+.

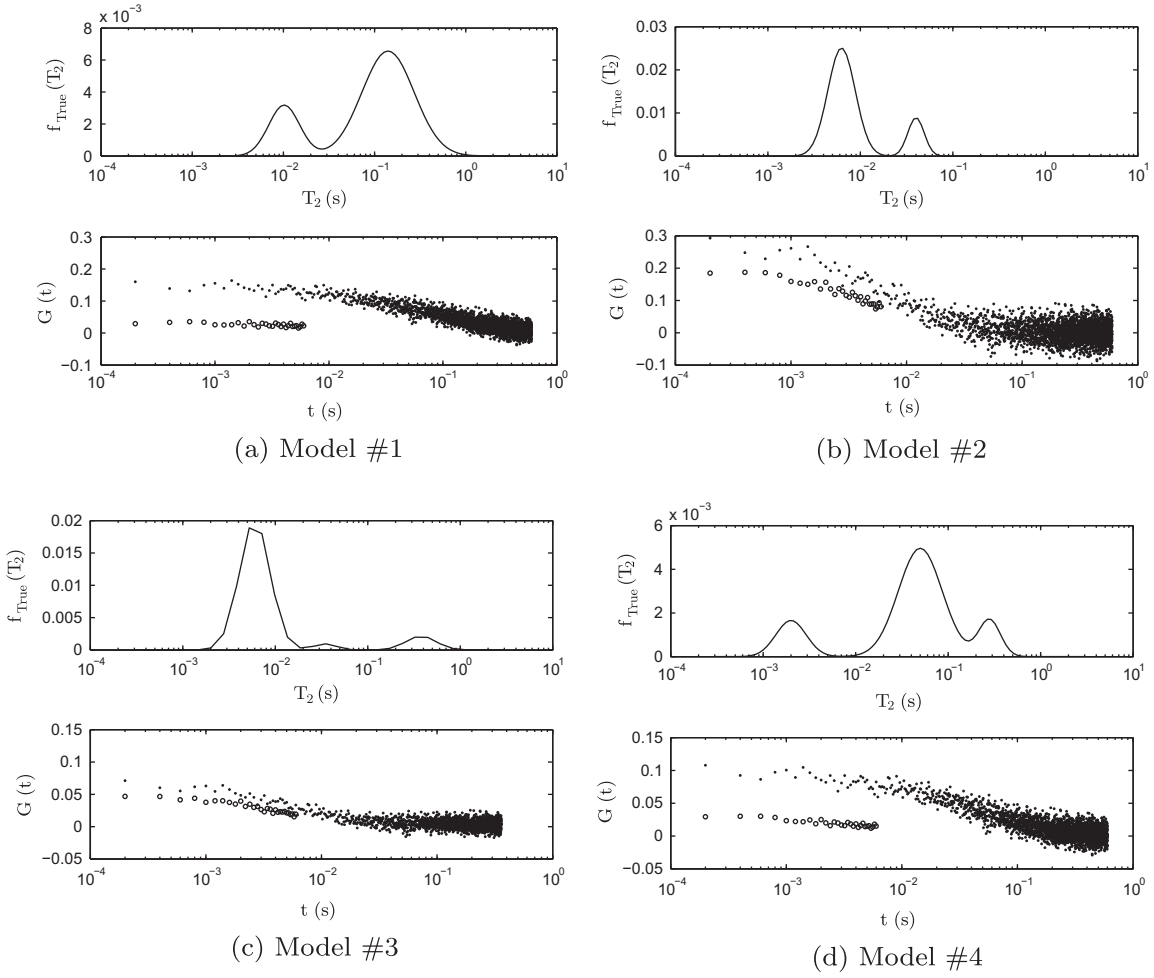

Fig. 2. Simulated T_2 distributions and noisy measurements used in benchmarking ILT and ILT+ algorithms.

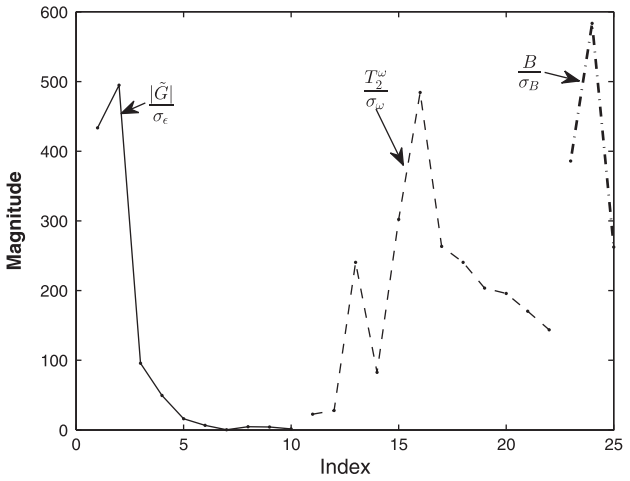

Fig. 3. Weighted terms used in ILT+ in Eq. (12).

$$(L)_{ij} = e^{-t_i/T_{2,j}}$$

representing the discretization of the forward mapping in (1). The matrix $\bar{L}$ is essentially the same matrix used in ILT but extended by the additional constraints. $K(T_c, T_2)$ represent the tapered Heaviside function varying smoothly between 0 and 1 with $K(T_c, T_2) = 0.5$ when $T_2 = T_c$ (see [6] for details). $T_{2,\min}$ and $T_{2,\max}$ represent the minimum and maximum value of the discretized T_2 vector.

W is the covariance matrix of uncertainties in the parameters

$$W = \begin{pmatrix} \frac{1}{\sigma_\epsilon} & & & & & \\ & \frac{1}{\sigma_{\omega_1}} & & & & \\ & & \ddots & & & \\ & & & \frac{1}{\sigma_{\omega N_m}} & & \\ & & & & \frac{1}{\sigma_{B_1}} & \\ & & & & & \ddots \\ & & & & & \frac{1}{\sigma_{B_{N_a}}} \end{pmatrix}$$

where σ_ϵ is the standard deviation of noise in the measurements and σ_{ω_i} and σ_{B_i} are the estimated uncertainties in the moments and areas estimated according to (11). In ILT this matrix is the identity because every measurement have the same uncertainty.

This method is applicable to data acquired from a variety of pulse sequences including CPMG, diffusion editing, inversion-recovery, saturation-recovery, and enhanced precision mode where the data are acquired at two different wait times. It is also possible to extend the algorithms to measurements where the

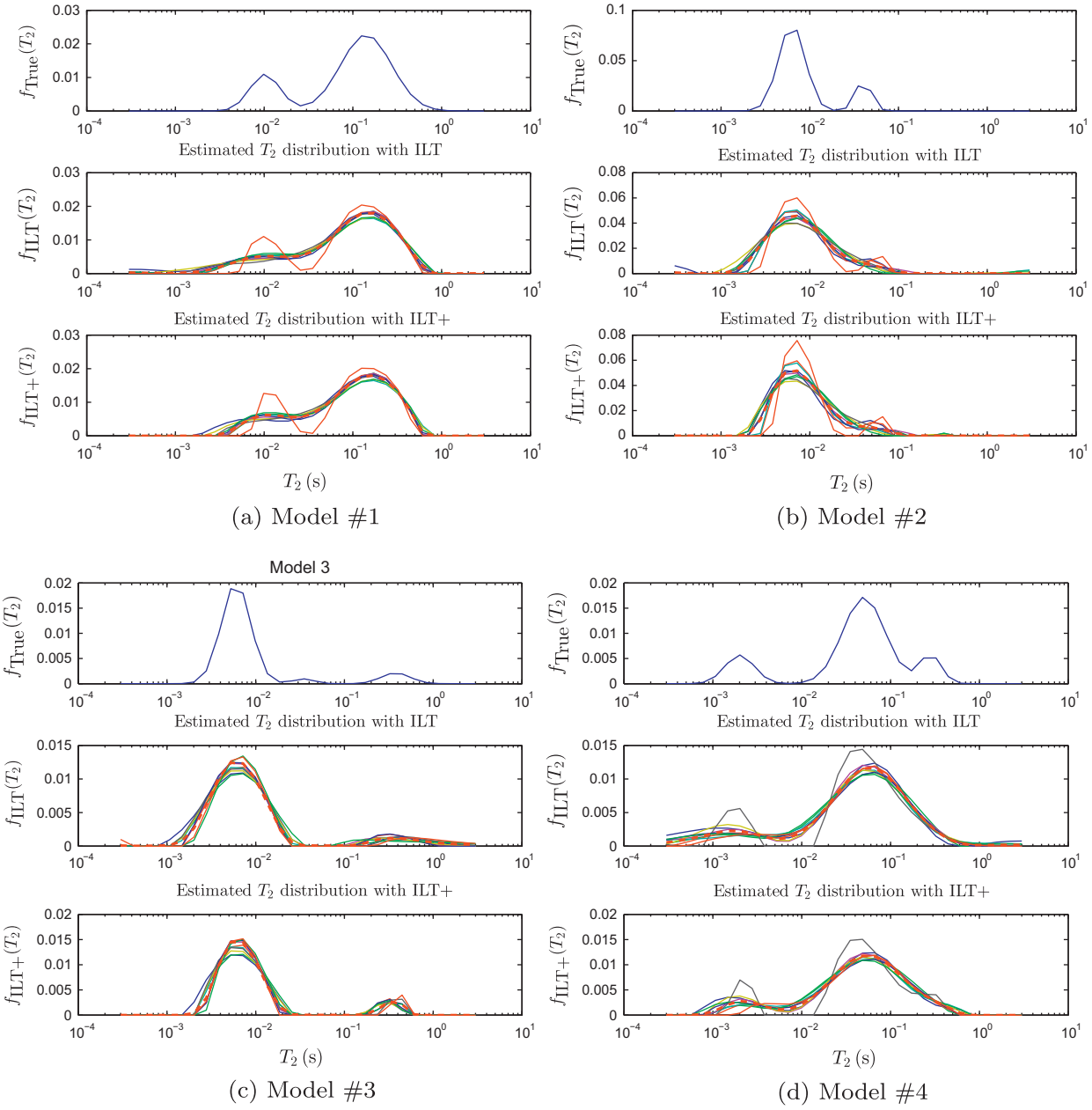

Fig. 4. Estimated T_2 distributions of the first 10 realizations. Red dashed line indicates the mean over all 100 realizations.

samples are not completely polarized (see [6] for a detailed discussion of this topic).

3. Simulation results

In this sub-section, we compare the performance of ILT+ and ILT on simulated data. The workflow comparing the two methods is shown in Fig. 1. The algorithm was benchmarked on simulated data obtained from T_2 distributions for the four models #1–4 shown in the top plot of Fig. 2. This are all T_2 distributions restricted to a region in T_2 spectra where the measuring tool is sensitive. The magnetization measurements $G(t)$ are generated according to (1). The measurements are then contaminated with additive white Gaussian noise with standard deviation per sample of $\sigma_\epsilon = 0.1$, with resulting signal-to-noise ratio SNR = 10. This SNR is representative of the poor quality SNR seen in downhole applications of NMR for characterization of porous media.

The bottom plots of Fig. 2 show the magnetization measurements for each model. These measurements are simulated at two different wait times with the following properties:

- two set of pulses are obtained at two different wait times and for different number of samples, indicated in the figure by black and white dots,
- the shorter pulse is repeated 10 times and averaged yielding a higher SNR.

The short pulse have the effect of improving the estimation of the T_2 distribution at short relaxation times.

For the long pulse, enough samples were taken to make sure the magnetization was completely decayed. This amounts to 3000 samples for models 1 and 2, 1800 samples for model 3, and 5000 samples for model 4. For the short pulse, the number of samples was fixed at 30. For both pulses the sample rate was 200 μs.

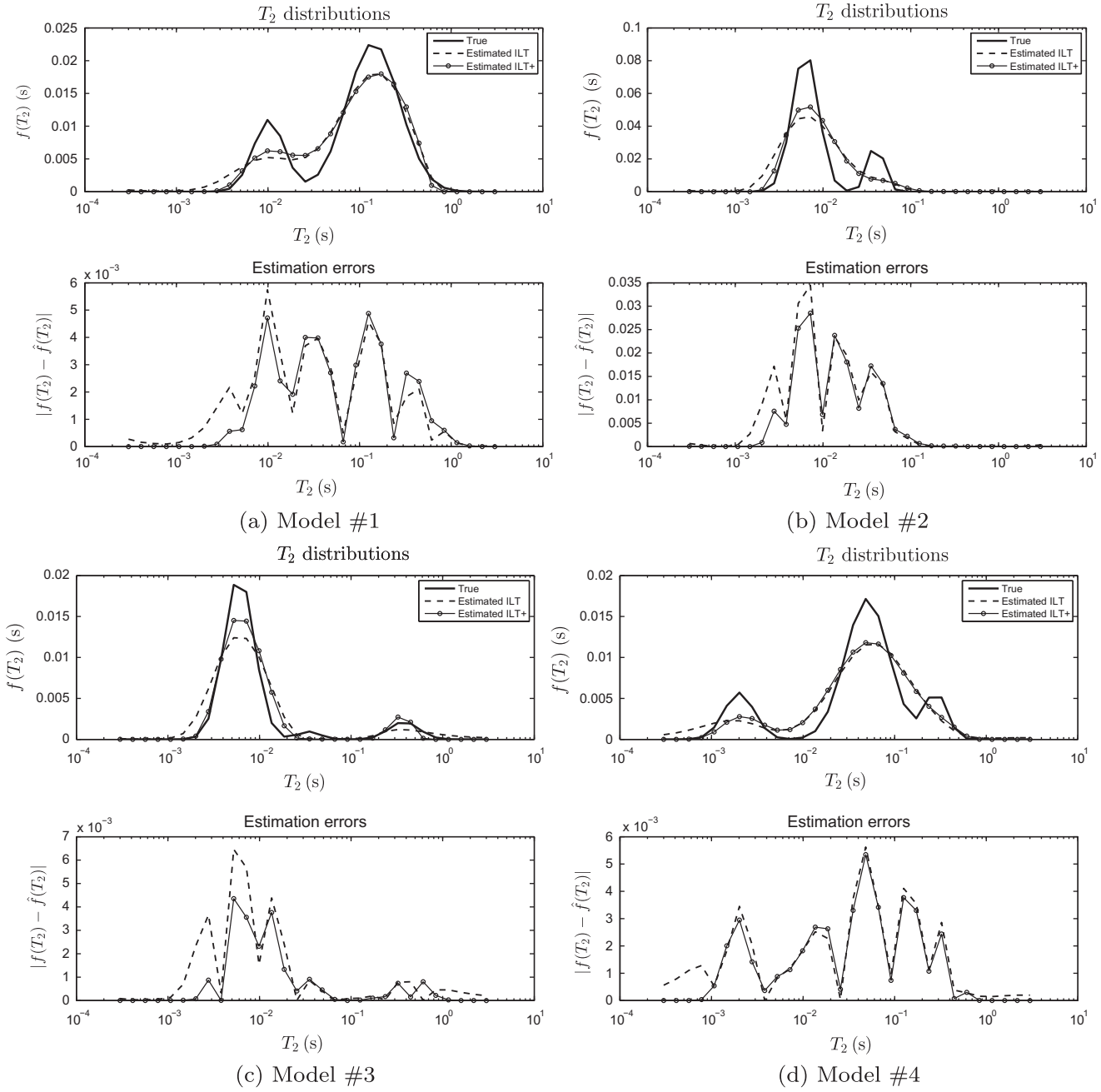

Fig. 5. Estimation errors using ILT and ILT+ to estimate the T_2 distributions. For each model the top plot shows the true T_2 distribution and the estimated T_2 distributions using ILT (dashed lines) and ILT+ (circles). The bottom plot shows the absolute error in the T_2 distribution estimation.

The noisy data are analyzed using the ILT and ILT+ algorithm described in this paper. For each realization, the same regularization parameter α was used in ILT and ILT+. The value of α was selected according to the Butler–Reed–Dawson algorithm [8] which tries to find an optimal amount of regularization based only on the data and the known noise variance. For each experiment and model the BRD algorithm select an different value for α. For instance, for model #4 after 100 noise realizations the value of α was 14 ± 8.9. For all cases, the area under the distribution, ϕ, is estimated according to the method described in [6].

The tapered areas B_i in (13) and the tapered transitions $K(T_2, T_{c_i})$ in (14) are calculated according to the exponential Haar transform in (9). The cutoff was set to $T_c = 0.01, 0.1,$ and 1 s . Also in (13) and (9) we estimate 12 moments with order ω between -0.5 and 1 by means of Eq. (6). The measurements were compressed using the truncated singular value decomposition and the number of singular values was selected to achieve a condition number (ratio between first singular value and last singular value used in the calculations) of 1000. Fig. 3 shows the weighted and compressed data (first 10 values), moments (next 12 values), and areas (last 3 values) in Eq. (12) for a typical case.

3.1. Increased resolution and reduction of artefacts

For each of the 100 realizations of the noisy data we estimate the T_2 distribution using ILT and ILT+. Fig. 4 shows the first 10 estimated T_2 distributions for each model. Also shown in thick dashed line is the mean over the 100 realizations. The results for models #1 and #4 illustrate an improvement in the resolution in the estimated T_2 distribution for $T_2 < 10$ ms. Model #3 shows an increase

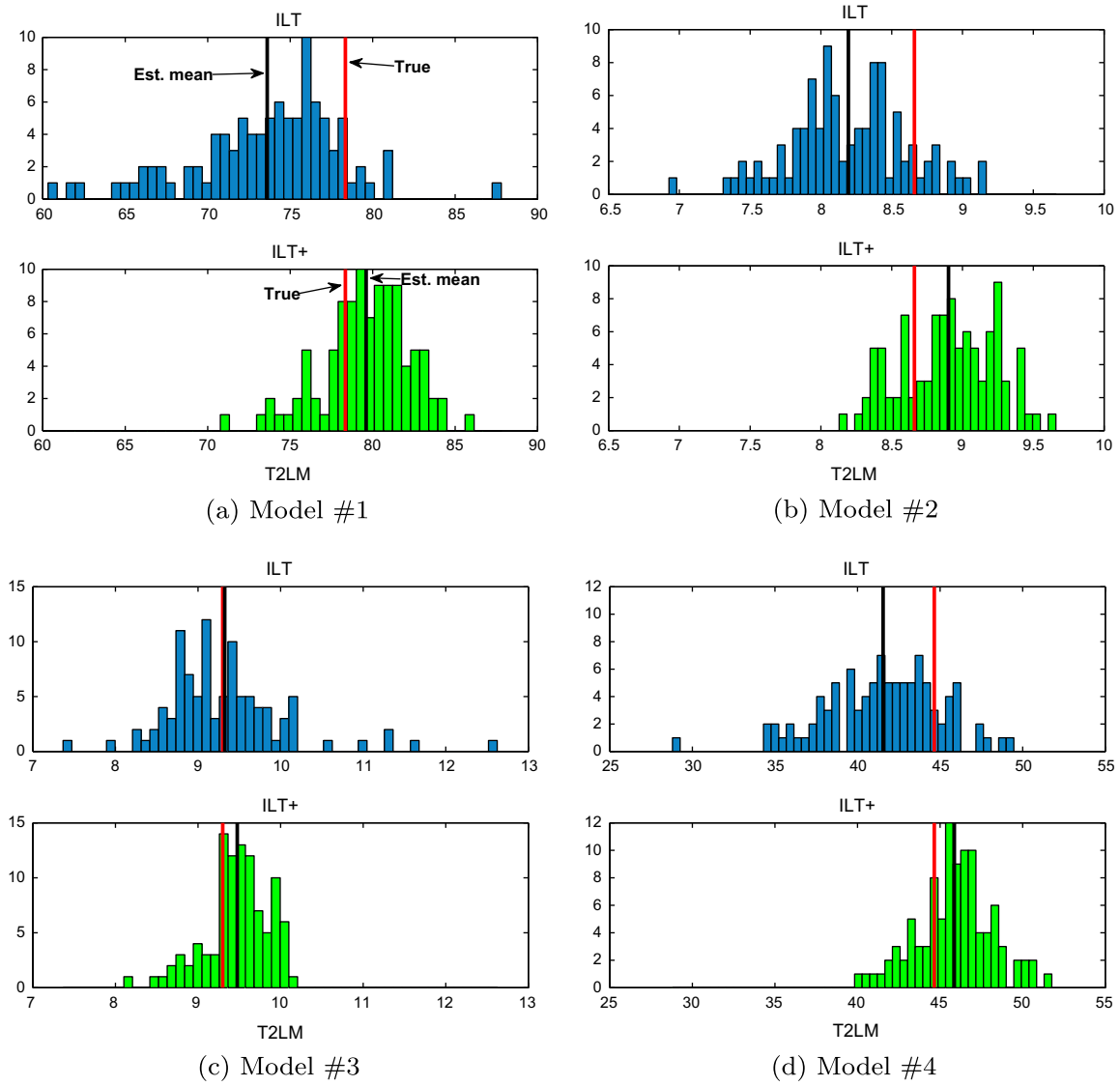

Fig. 6. Histogram of estimated T2LM for a SNR = 10 and 100 realizations.

Table 1
Estimation of petrophysical parameters. SNR = 10.

Models	True	ILT		ILT+	
		$\mu \pm \sigma$	nrmse (%)	$\mu \pm \sigma$	nrmse (%)
(a) Comparison of estimated T2LM (ms)					
1	78	74 ± 4.51	8.3	80 ± 2.61	3.7
2	8.7	8.2 ± 0.417	7.2	8.9 ± 0.33	4.7
3	9.3	9.3 ± 0.754	8.1	9.5 ± 0.391	4.6
4	45	35 ± 3.43	22	40 ± 3.04	12
(b) Comparison of estimated BFV					
1	0.035	0.035 ± 0.00225	6.4	0.033 ± 0.0019	8.2
2	0.24	0.27 ± 0.00721	11	0.25 ± 0.00672	6.9
3	0.061	0.064 ± 0.00203	6.7	0.061 ± 0.00158	2.6
4	0.024	0.035 ± 0.00284	50	0.033 ± 0.00292	42

in resolution for $T_2 > 0.1$ s. In all cases we see a reduction in artefacts at the beginning and end of the T_2 spectrum. The improvement in the estimation of the T_2 distribution is shown more explicitly in Fig. 5 which shows the absolute estimation errors of the T_2 distribution. The plots illustrate a reduction in error specially at short relaxation times.

3.2. Estimation of petrophysical parameters

With the estimated T_2 distribution we can calculate petrophysical parameters like the logarithmic mean (T2LM) and the bound fluid volume (BFV) defined as

$$BFV = \int_0^{T_c} f(T_2) dT_2$$

where we have chosen a value of $T_c = 33$ ms which is a typical value for this parameter [1]. Fig. 6 shows the histogram of the estimated T2LM using ILT and ILT+. The ILT+ estimates tend to be less spread out (less standard deviation) when compared to ILT and the mean (black line) tends to be closer to the true value (red line) in most cases (smaller bias). This behavior is confirmed by looking at Table 1a where μ indicates the mean of the estimate, σ indicates the standard deviation, and nrmse is the normalized root mean square error defined for any estimate *Est* as

$$nrmse = \frac{\sqrt{\langle (Est - \text{True value})^2 \rangle}}{\text{True value}} \times 100$$

where $\langle \cdot \rangle$ represents the mean.

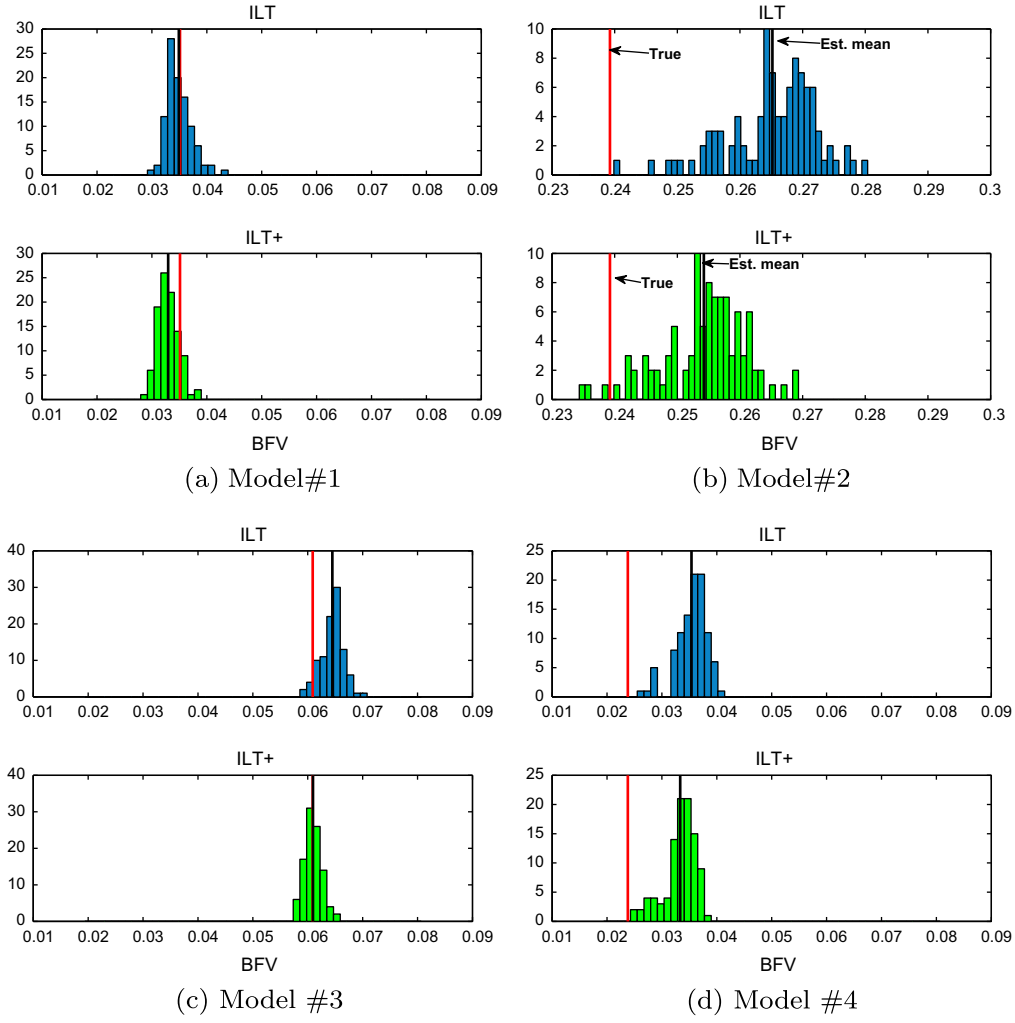

Fig. 7. Histogram of estimated BFV for a SNR = 10 and 100 realizations.

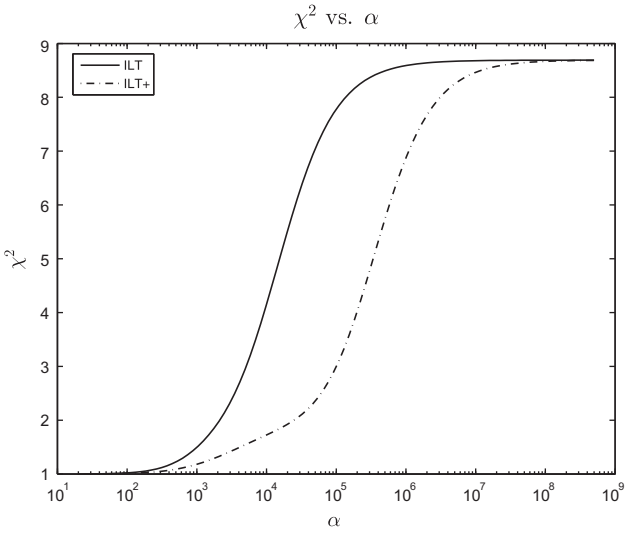

Fig. 8. χ^2 vs. α for model #1 and a SNR = 10.

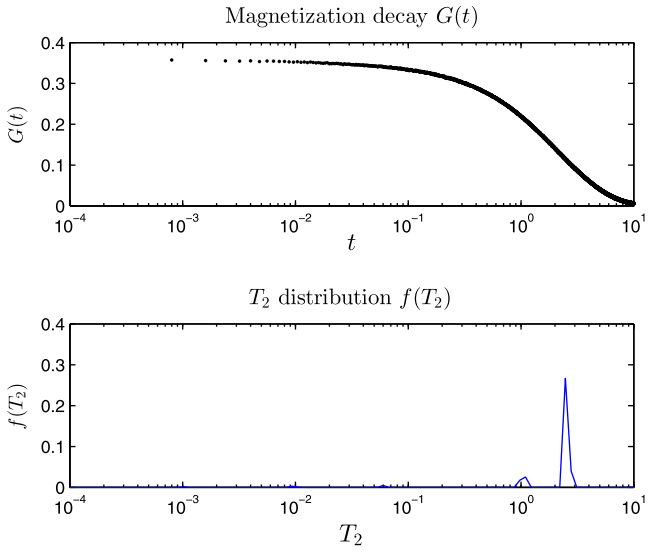

Fig. 9. Ground truth obtained from averaging 10 laboratory experiments for the same sample. Top plot shows the magnetization decay while the bottom plot shows the T_2 distribution.

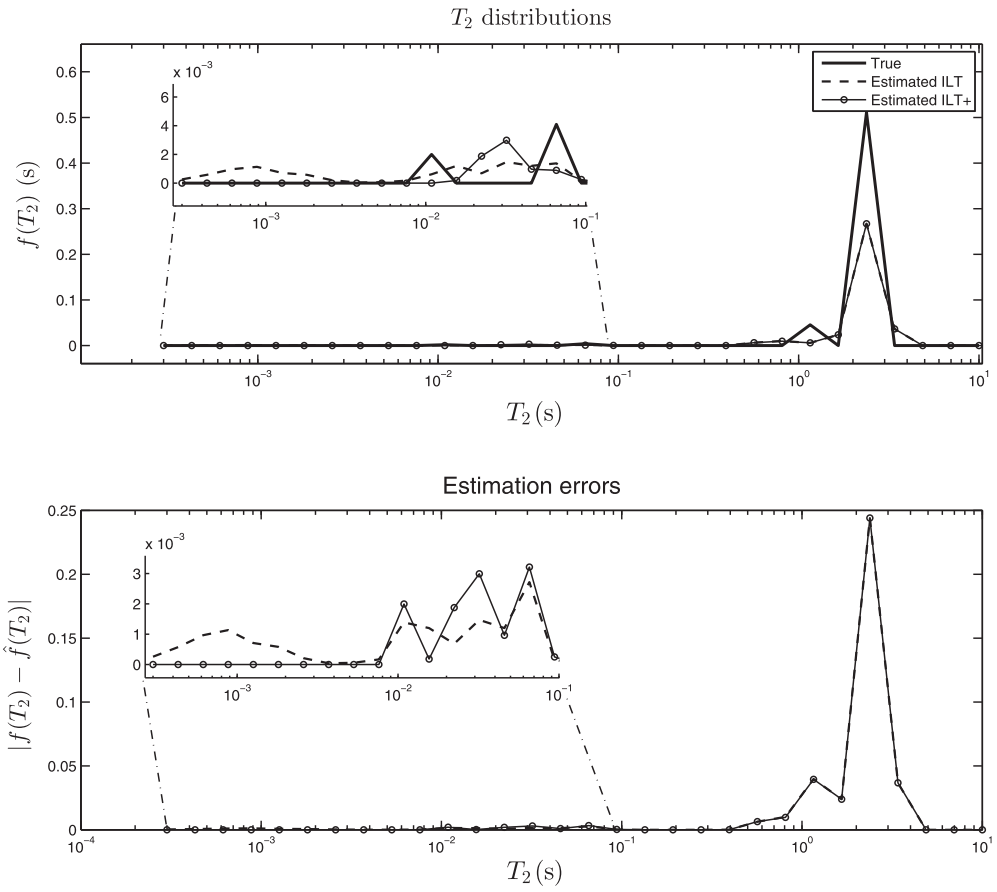

Fig. 10. Top plot shows the estimated T_2 distribution using ILT and ILT+ as well as the true value.The bottom plot shows absolute error in the estimation of the T_2 distribution.

Table 2
Estimation of petrophysical parameters of experimental data.

Parameter	True	ILT		ILT+	
		$\mu \pm \sigma$	nrmse (%)	$\mu \pm \sigma$	nrmse (%)
T2LM (ms)	1986	1881 ± 104.8	7.27	2069 ± 54.53	4.92
BFV	0.00963	0.0114 ± 0.002926	34.2	0.007145 ± 0.0007663	26.9

Similar results were obtained for the BFV estimates as illustrated in Fig. 7 and Table 1b.

3.3. Dependence on regularization

Finally, it was found that the addition of linear functionals as constraints to the estimation of the T_2 distribution reduces the dependence of the fit error on the regularization parameter α. Let $\chi^2_{ILT} = \|G - Kf_{ILT}\|^2$ be the error in the fit obtained from using the T_2 distribution f_{ILT} estimated by using ILT and $\chi^2_{ILT+} = \|G - Kf_{ILT+}\|^2$ the corresponding error in the fit using the ILT+ T_2 distribution, $f_{ILT+}(T_2)$. Fig. 8 shows the fit error as a function of α for the two methods. In this example, the data is obtained from model #1 with SNR = 10. It is observed that the fit error is independent of α for a larger range when using ILT+.

4. Experimental validation

In order to validate the algorithms on real measurements we ran 10 laboratory experiments on a doped water sample (water and salt). We averaged the 10 magnetization measurements to obtain a very high signal-to-noise ratio signal. This high quality measurement was processed to obtain the "ground truth" using ILT (see Fig. 9). Then the 10 individual measurements were processed with ILT and ILT+ and compared to the ground truth. Fig. 10 shows the estimated T_2 distributions as well as the absolute error with respect to the ground truth. It was found that the two estimates where equivalent for $T_2 > 0.1$ s. However, there were some differences for $T_2 < 95$ ms. Therefore, we estimated the BFV for a cutoff $T_c = 95$ ms. Table 2 shows the mean, standard deviation, and nrmse of the estimated T2LM and BFV. As shown in this table both parameter were estimated with a reduced nrmse with ILT+ as compared to ILT.

5. Summary

We have presented a new algorithm for the estimation of a T_2 distribution that is consistent with the measurements and is constrained by linear functionals of the data that can be directly estimated from the measurement by integral transforms. Specifically, the moments and areas estimated directly from the data are used

as constraint. These constraints can be justified by noting that they are related to important physical properties like permeability and hydrocarbon viscosity. In general, we find that this new algorithm is less sensitive to regularization. Simulation results also show an increase in resolution of some of the features of the T_2 distribution as well as a reduction in the artefacts in the inversion leading to smaller bias and variance in the estimated parameters.

References

[1] R.L. Kleinberg, C. Straley, W.E. Kenyon, R. Akkurt, S.A. Farooqui, Nuclear magnetic resonance of rocks: T_1 vs. T_2, SPE 26470 (1993) 553–563.
[2] L. Venkataramanan, Y.-Q. Song, M.D. Hürlimann, Solving Fredholm integrals of the first kind with tensor product structure in 2 and 2.5 dimensions, IEEE Trans. Signal Process. 50 (2002) 1017–1026.
[3] J.G. McWhirter, E.R. Pike, On the numerical inversion of the Laplace transform and similar Fredholm integrals of the first kind, J. Phys. A: Math. Gen. 11 (1978) 1729–1745.
[4] C.L. Epstein, J. Schotland, The bad truth about Laplace's transform, SIAM Rev. 50 (2008) 504–520.
[5] W.H. Press, S.A. Teukolsky, W.T. Vetterling, Numerical Recipes in C, Cambridge University Press, 1992.
[6] F.K. Gruber et al., Estimation of petrophysical and fluid properties using integral transforms in nuclear magnetic resonance, J. Magn. Reson. 228 (2013) 104–115.
[7] L. Venkataramanan, F.K. Gruber, T.M. Habashy, D.E. Freed, Mellin transform of CPMG data, J. Magn. Reson. 206 (2010) 20–31.
[8] J.P. Butler, J.A. Reeds, S.V. Dawson, Estimating solutions of the first kind integral equations with nonnegative constraints and optimal smoothing, SIAM J. Numer. Anal. 18 (3) (1981) 381–397.